POLITECNICO DI TORINO
Repository ISTITUZIONALE

Impact of Correlated Mobility on Delay-Throughput Performance in Mobile Ad-Hoc Networks

Original
Impact of Correlated Mobility on Delay-Throughput Performance in Mobile Ad-Hoc Networks / Ciullo, D., Martina, V., Garetto, M., Leonardi, E.. - (2010). (IEEE INFOCOM 2010 San Diego (CA), USA March 15-19, 2010).

Availability:
This version is available at: 11583/2298243 since:

Publisher:

Published
DOI:

Terms of use:

This article is made available under terms and conditions as specified in the corresponding bibliographic description in the repository

Publisher copyright

(Article begins on next page)

11 September 2026

Parametric Design Method for SPM Machines Including Rounded PM Shape

Chao Lu, Simone Ferrari, and Gianmario Pellegrino
Department of Energy
Politecnico di Torino, Turin, Italy
chao.lu@polito.it
simone.ferrari@polito.it
gianmario.pellegrino@polito.it

Claudio Bianchini, and Matteo Davoli
DISMI
University of Modena and Reggio Emilia, Italy
claudio.bianchini@rawpowergroup.it
matteo.davoli@unimore.it

***Abstract*- Surface-mounted permanent magnet (SPM) machine is widely applied in industry application because of its high torque density, high efficiency and simple rotor structure. This study presents a parametric design plane, which makes the desired machine performance visualized during the machine design process. Based on that, a new parametric design method is introduced to simplify the design procedure of SPM motors. Besides the standard radial PM shape, the presented method applies to magnets of modified shape called "rounded", intended for torque ripple minimization at no additional manufacturing cost and such as stator skewing, rotor stepping or the like. The design flowchart for the method is illustrated and the output designs are validated by finite element analysis (FEA) and experimental tests. The proposed design method is embedded in a machine design instrument available online.**

***Key words*— Parametric design, SPM Machine, Rounded PM Shape, Torque ripple, Cost reduction**

I. Introduction

Permanent magnet synchronous machines (PMSMs) have attracted substantial research interests during last decades due to their high torque density, high efficiency and fast dynamic performance. Among PMSMs, surface-mounted permanent magnet (SPM) machines are popular in industrial application for their simple rotor construction. Caused by interaction between permanent magnet (PM) and slotted stator structure [1], the cogging torque of SPM motors is considerable, inducing vibrations and noise particularly at low speed. Under load, torque ripple arises, with similar side effects. Various solutions have been proposed to reduce cogging torque and torque ripple, such as skewing [2], shifting PMs [3], etc.

A general design approach for SPM motors has been illustrated in [4]. A parametric design technique for SPM motors with concentrated windings has been proposed in [5]. Inspired by [4]-[5], this research proposes a new parametric design method for SPM motors with distributed windings. A new parametric design plane, built on rotor-stator radius split and magnet-airgap length ratio, is introduced. During the design process, the machine torque capability and power factor (PF) at rated current condition are represented on the parametric plane. The key geometric quantities of the candidate machine are found by selecting the desired torque and PF performance point on the plane. A two-dimensional machine model will be automatically built, ready for finite-element analysis (FEA) verification. In addition, the new method is also suitable for motors with modified PM shape [6] by introducing a magnet shaping factor, resulting in the possibility of torque ripple and cost optimization. The demagnetization limit at the edges of PMs is analyzed. Besides, PM quantity is also considered to decrease the cost. The new parametric design procedure simplifies the machine design process for SPM motors, including rounded PM shape, covering abundant magnetic calculations. The design method is integrated in machine design software available online [7], which contains sizing equations, and magnetic static FEA [8].

Four SPM motors with same stator structure are designed via the presented parametric method. Two of them have standard radial PMs, and the other two have optimized rounded shapes, respectively. The motor performance results are validated through both FEA simulations. Experimental results are presented for one of the optimized designs.

II. Design Procedure

A. Reference data

This study uses the same stack dimensions and slots-poles combinations as the previous work [6]. The key specifications are reported in Table I.

B. Rotor geometry

The cross section view of an SPM rotor with rounded magnets is reported in Fig.1. The outer profile of the PM is rounded shaped and follows the set of parameters defined in the figure. l_m is the maximum magnet length at the center of the pole (along with d axis), r is the rotor core radius, β is the magnet length at the magnet edge, in p.u. of l_m. When β equals to 1, the magnet length at edge equals l_m and the PM shape becomes uniform. α_m is the magnet angular span, ξ is the rotor angular coordinate, starting from the magnet center line, $g(\xi)$ is the airgap length function of ξ and r_c is the radius of the outer rounded magnet profile. After defining the magnet parameters (α_m, l_m and β), the magnet length distribution $l_m(\xi)$, $g(\xi)$, r_c and central position $O'$of rounded profile are

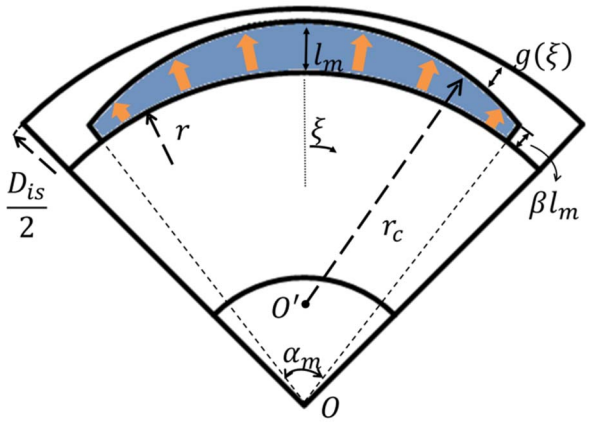

Fig. 1. Definition of design parameters for SPM motors with rounded PM shape

TABLE I RATINGS OF THE MACHINE

PARAMETERS	UNITS	VALUES
Pole pairs (p)		3
Stator slots (q)		36
Stator outer diameter (D)	mm	175
Length (L)	mm	110
Copper loss	W	550
Thermal loading ($\boldsymbol{k_j}$)	kW/m^2	9.1
Minimum airgap length	mm	1
Copper filling factor		0.432
Steel grade		M600-50A
Steel loading ($\boldsymbol{B_{fe}}$)	T (pk)	1.5
PM grade		NdFeB 32 MGOe
Remanence ($\boldsymbol{B_r}$)	T	1.16
Rated current	A	25
Number of turns per phase ($\boldsymbol{N_s}$)		120
Resistance (phase to phase)	[Ω]	0.835
Torque target	Nm	50
Torque ripple target	Nm	2

calculated.

C. Airgap Flux Model

Assuming that the cross sectional areas of PMs and external circuit are equal [9], for a slotless machine with radially magnetized PMs, it is obtained that,

$$B_g(\xi) \cong B_m(\xi) = \frac{l_m(\xi)/g(\xi)}{l_m(\xi)/g(\xi)+k_c\cdot\mu_r}\cdot B_r \quad (1)$$

Here $B_m(\xi)$ is the magnet flux density function, k_c is the Carter coefficient, and μ_r is the relative permeability of the magnet, and B_r is the magnet remanent flux density.

Based on the magnet parameters input (l_m, α_m and β), the radius of rounded magnet shape r_c can be achieved as,

$$r_c = \frac{\left(2r^2+2l_m r(\beta+1)\right)\left(1-\cos\frac{\alpha_m}{2}\right)+(\beta^2+1-2\beta\cos\frac{\alpha_m}{2})l_m^2}{2\left(r\left(1-\cos\frac{\alpha_m}{2}\right)+l_m(1-\beta\cos\frac{\alpha_m}{2})\right)} \quad (2)$$

Then, the magnet length expression $l_m(\xi)$ can be got according to the PM positions,

$$l_m(\xi) = (r + l_m - r_c)\cos\xi - r + \sqrt{r_c^2 - ((r+l_m)sin\xi - r_c sin\xi)^2} \quad (3)$$

The relationship among stator inner diameter D_{is}, $l_m(\xi)$ and $g(\xi)$ is given as,

$$l_m(\xi) + g(\xi) + r = D_{is}/2 \quad (4)$$

Then substituting (3) into (4), the airgap length function is then calculated as,

$$g(\xi) = D_{is}/2 - (r + l_m - r_c)\cos\xi - \sqrt{r_c^2 - ((r+l_m)sin\xi - r_c sin\xi)^2} \quad (5)$$

Combining equations (3) to (5), the airgap flux density expression $B_g(\xi)$ can be expressed as,

$$B_g(\xi) = [(r + l_m - r_c)\cos\xi - r + \sqrt{r_c^2 - ((r+l_m)sin\xi - r_c sin\xi)^2}]\cdot B_r/ [(1-k_c\mu_r)(r+l_m-r_c)\cos\xi - r + \frac{k_c\cdot\mu_r D_{is}}{2} + (1-k_c\mu_r)\sqrt{r_c^2 - ((r+l_m)sin\xi - r_c sin\xi)^2}] \quad (6)$$

Three cases of airgap flux density distribution $B_g(\xi)$ waveforms are reported in Fig. 2. The analytical results are presented in continuous lines and the circle marked points represent the FEA results. It can be seen that the analytical results agree with the FEA results along with the PM areas. Nonetheless, influenced by fringing effect, in the regions without PMs, the flux density cannot vanish, as indicated by the FEA results. The proposed mathematical model (6) assumes the airgap flux density to be zero off the magnet pole, with minor effect on torque and PF prediction.

The fundamental component's amplitude B_{g1} is obtained by Fourier transform of the analytical flux density distribution $B_g(\xi)$ over one pole pair. The magnet flux linkage λ_m is evaluated considering the fundamental component of the airgap flux density and neglecting higher order harmonics. Then λ_m is calculated by,

$$\lambda_m = \frac{2(r+l_m+g)LN_s k_w B_{g1}}{p} \quad (7)$$

Where p is the number of pole pairs, L is the machine

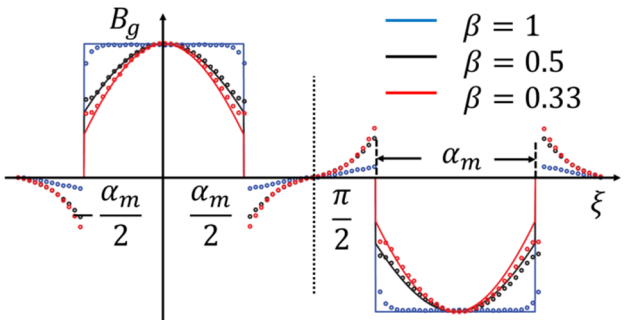

Fig. 2. Airgap flux density distribution of a slotless motor, analytical results: continuous lines; FEA results: circle marked

length, N_s is the number of turns per phase and k_w is the winding factor. Table II summarizes the difference between analytical and FEA results on B_{g1} and λ_m. The agreement of the results is reasonably good for all considered values of the parameter β.

D. Design Inputs

With reference to the machine's ratings reported in Table I, the slot-pole combination is constant in this study and the initial design inputs are:

- Stack dimensions *D, L* and minimum airgap length *g*.
- PM remanence B_r and peak flux density in steel B_{fe}.
- Thermal loading k_j.

The number of turns N_s is set to an initial value and adjusted in the final stages of the design according to the specified voltage and speed ratings.

The thermal loading k_j [W/m^2] is expressed in the form of copper loss per stack surface:

$$k_j = \frac{Copper\ loss}{\pi DL} = \frac{(6N_sI)^2}{\frac{k_{Cu}}{\rho}\frac{L}{L+l_{end}}\cdot 2\pi D\cdot A_{slots}} \tag{8}$$

Where D is the machine outer diameter, A_{slots} is the total slot areas, k_{Cu} is the copper filling factor, l_{end} is the end-turn length, I is the amplitude of current and ρ is the resistivity of copper.

After defining the size and winding type, the allowed electric loading A_s [A/m] is indirectly obtained by the thermal loading (8),

$$A_s = \frac{6N_sI}{2\pi(r+l_m)} \tag{9}$$

The product N_sI together is proportional to $\sqrt{k_j}$ according to (8), and also contributes to electric loading A_s.

Thermal loading k_j, instead of A_s, is used here because it contains information both on stator and rotor quantities, whereas the electric loading refers to the rotor size only.

TABLE II COMPARISON BETWEEN MODEL AND FEA

$l_m = 4.5\ mm$, $g_{min} = 1\ mm$, $\alpha_m = 171°$	β	0.33	0.5	1
B_{g1} [T]	Model	0.98	1.02	1.16
	FEA	1	1.04	1.15
	Error	-2 %	-2 %	0.8 %
λ_m [Vs]	Model	0.47	0.49	0.55
	FEA	0.47	0.49	0.53
	Error	0 %	0 %	3.7 %

Moreover, k_j is more intimately related to the copper temperature.

E. Design plane: T and PF versus x and l_m/g

The torque-PF design plane is defined after the two key factors of SPM motor, x and l_m/g. x is defined as the split ratio of the machine,

$$x = \frac{r+l_m}{R} \tag{10}$$

Where R is the stator outer radius, and $r + l_m$ is the rotor plus magnet outer dimension. From (1), the airgap flux density distribution $B_g(\xi)$ directly refers to the magnet on airgap ratio l_m/g. Therefore, x and l_m/g together determine $B_g(\xi)$, B_{g1} and λ_m, according to (6) and (7).

Afterwards, the stator geometry is dependent on the ratio of $B_g(\xi)$ to steel loading B_{fe}. Since B_{fe} is defined at the beginning (1.5 T for standard silicon steel type), the dimension of tooth width and yoke length can be achieved as the product of average $B_g(\xi)$ and x,

$$w_t = \frac{\pi D}{6pqB_{fe}}(x \cdot B_{g_avg}) \tag{11}$$

$$l_y = \frac{\pi D}{4pB_{fe}}(x \cdot B_{g_avg}) \tag{12}$$

Where q is the number of slots per pole per phase, B_{g_avg} is the average value of $B_g(\xi)$. The detailed stator geometry definition is shown in Fig. 3.

F. Torque and Power Factor Expressions

With the current is controlled on the q axis, torque can be expressed as,

$$T = \frac{3}{2}p\lambda_m i_q \tag{13}$$

From (8), it is known that the current amplitude is a function of the thermal loading factor, the motor dimensions and the number of turns, shown as,

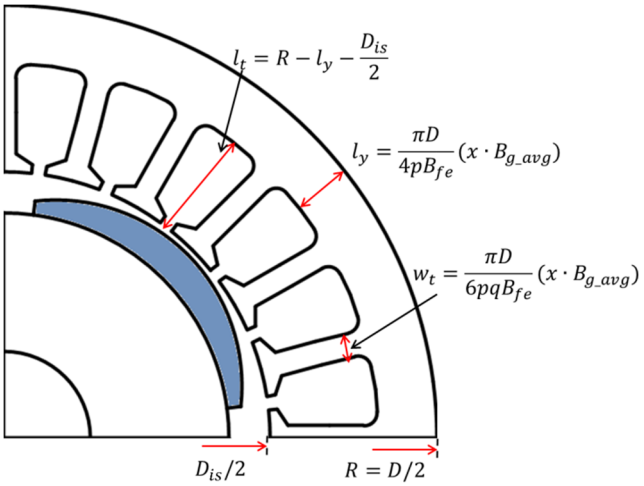

Fig. 3. Stator geometry definition

$$i_q = I = \frac{1}{6N_s}\sqrt{k_j \cdot (\frac{k_{Cu}}{\rho}\frac{L}{L+l_{end}} \cdot 2\pi D \cdot A_{slots})} \quad (14)$$

The two factors A_{slots} and l_{end} in (14) are the function of x and B_{g1}. The other inputs k_j, k_{Cu}, ρ, D and L are specified in Table I. Larger x will result in smaller slot area, and vice versa. In addition, larger B_{g1}, results from higher value of l_m/g, will also indirectly decrease the slot area A_{slots}, because ticker teeth and back iron would be associated to a larger airgap flux. The situation for l_{end} is as same as A_{slots}, because shorter slots have shorter end-turn length, as reported in (15),

$$l_{end} = \frac{(D_{is}+5l_t)\pi}{pq} \quad (15)$$

Where l_t is the tooth length shown in Fig. 3. The relationship among l_t, l_y and D_{is} is presented as,

$$l_t + l_y + \frac{D_{is}}{2} = R \quad (16)$$

With the current on the q axis, then PF is defined as:

$$PF = \cos(\varphi) \cong \frac{\lambda_m}{\sqrt{{\lambda_m}^2+(L_q i_q)^2}} \quad (17)$$

Where $L_q = L_d = L_s$, for SPM motor, can also be expressed as a function of x and l_m/g. The equation for L_q has been illustrated in [5], and repeated here. The total inductance consists of magnetizing inductance L_m, plus the slot leakage inductance L_{slot} and the tooth tip leakage inductance L_{tip} [10]:

$$L_m = \frac{3}{2}\cdot\frac{8}{\pi}\cdot(\frac{k_w N_s}{p})^2 \cdot \mu_0 \cdot L \cdot \frac{Dx/g}{l_m/g+k_c} \quad (18)$$

$$L_{slot} = \frac{12}{6pq}\cdot k_s \cdot \mu_0 \cdot L \cdot {N_s}^2 \quad (19)$$

$$L_{tip} = \frac{12}{6pq}\cdot k_t \cdot \mu_0 \cdot L \cdot {N_s}^2 \quad (20)$$

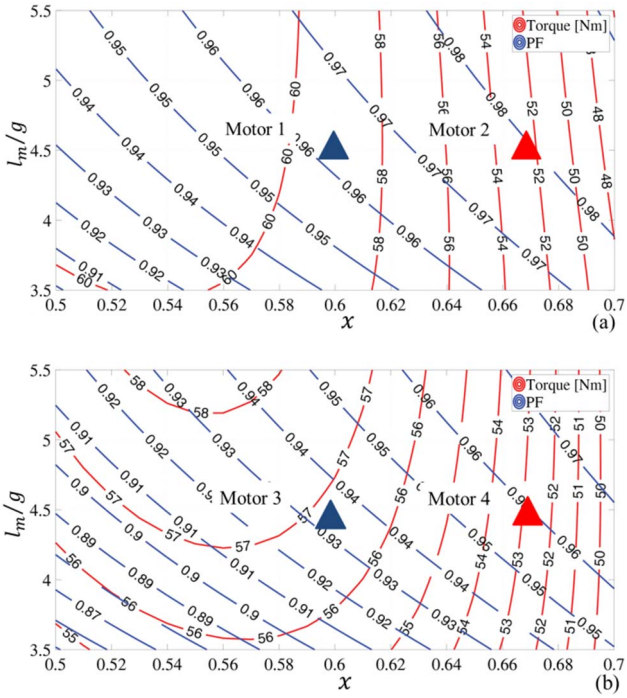

Fig. 4. Torque and PF design plane, $\alpha_m = 171°$, (a). $\beta = 1$, (b). $\beta = 0.33$

Here, k_s and k_t are permeance factors for slot leakage inductance and tooth tip leakage inductance respectively, dependent on slot shape [10]. Then L_q is the sum of the three portions,

$$L_q = L_m + L_{slot} + L_{tip} \quad (21)$$

Integrating (7), (14), (17) and (21), PF can be calculated in the form of x and l_m/g. Finally, the torque and PF plane can be established according to (13) and (17).

G. Results

Two plane examples are reported in Fig. 4. Subcase (a) refers to radial magnets with uniform length ($\beta = 1$), case (b) has $\beta = 0.33$. For both planes, α_m is set as 171°. Each point on this plane represents one motor design. One design can be selected according to the desired torque and PF output. After one point is picked from the plane, one motor model will be automatically built, on the basis of the equations described above. FEA validation follows, to verify whether the motor is in line with the specified performance. The detailed design flowchart is reported in Fig. 5.

After FEA validation at rated current condition, if the torque result is not adequate for the target, stack size or thermal loading can be improved to increase the torque generation. Meanwhile, if the torque ripple is still high, reducing β or finding better PM angular span α_m is needed. Then the process is repeated.

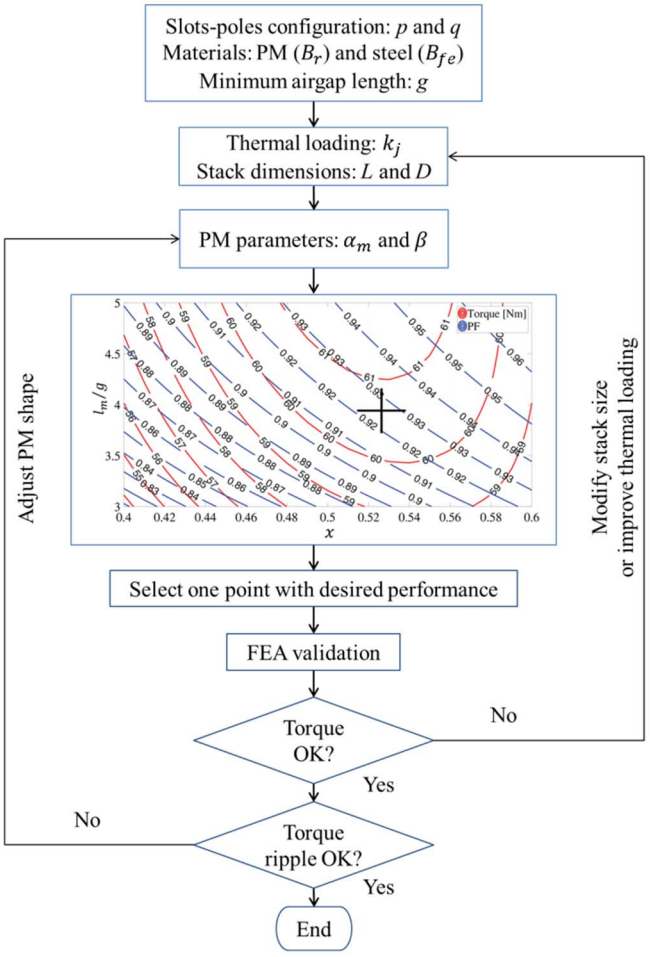

Fig. 5. Flowchart of the design procedure

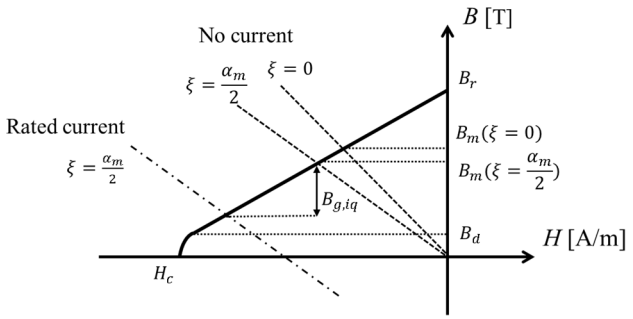

Fig. 6. Operating point determination with demagnetization limit (NdFeB 32 MGOe @80 °C)

H. Demagnetization limit

The PM ends should not be too thin to prevent fractures in the manufacturing process and demagnetization. The PM ends are vulnerable to demagnetization risk, compared with PM center both for their reduced length and for the effect of the stator current aligned with the q axis, whose magneto motive force (mmf) has the peak value in the area of minimum magnet thickness. Therefore, the edge length must be lower constrained by means of the parameter β. The maximum armature mmf per pole is defined as [9],

$$F_{p1} = \frac{3}{2}\frac{4}{\pi}\frac{k_w N_s}{2p} i_q \tag{22}$$

Assuming that the iron has infinite permeability and all the mmf drop happens at the airgap, the maximum airgap flux density produced by current alone at the magnet's edges is,

$$B_{g,iq} = \frac{F_{p1}\mu_0}{g} = \frac{3}{2}\frac{4}{\pi}\frac{\mu_0 k_w N_s}{2p[l_m(\xi=\frac{\alpha_m}{2})+\mu_r k_c g(\xi=\frac{\alpha_m}{2})]} i_q \tag{23}$$

To protect the PMs, they must be designed so that the flux density (23) is equal or larger than the minimum allowed flux density of the PMs B_d, corresponding to the knee point of the magnet demagnetization curve. Hence,

$$B_m(\xi = \frac{\alpha_m}{2}) \geq B_{g,iq} + B_d \tag{24}$$

The *B-H* curve and the relationship (24) are graphically associated in Fig. 6. In this study, B_d is 0.1 T and the maximum allowed current I_{max} is 26 A. Moreover, Fig. 7 represents the relationship among maximum allowed current and β, with l_m as a parameter. The figure illustrates that the maximum current is proportional to the shaping factor β when l_m is fixed. For this design, acceptable values of β are above 0.30.

III. Design Example and Results

The proposed parametric method is tested here by comparing the outcome of analytical calculation in the parametric plane (Fig. 4) with FEA simulation and experimental results. Two designs are built from Fig.4a, having uniform magnet length. Other two designs are created from Fig. 4b, with rounded magnet shape ($\beta = 0.33$), using the same x and l_m/g combinations used for the previous designs, with uniform length.

A. Design cases

Fig. 8 presents the structure of the four models selected from each design plane reported in Fig. 4. It is obvious from Fig. 8 that as x grows up, slot area becomes smaller when l_m/g is kept constant (from Motor 1 to Motor 2, and Motor3 to Motor 4). Considering the same x and l_m/g combination, rounded motors will have shorter stator yoke and tooth width, since their B_{g1} are less than those of uniform length motors (comparing Motor 1 with Motor 3, or Motor 2 with Motor 4). It is emphasized here that although the PM quantity is reduced from Motor 2 to Motor 4 due to the magnet shaping, the slot area is increased, thereby improving electric loading A_m and rated current. Consequently, the nominal torque produced by Motor 4 is greater that Motor 2, despite of lower PM volume.

B. FEA simulation results

All the models are evaluated under each rated condition via FEA simulations. Results comparison between parametric

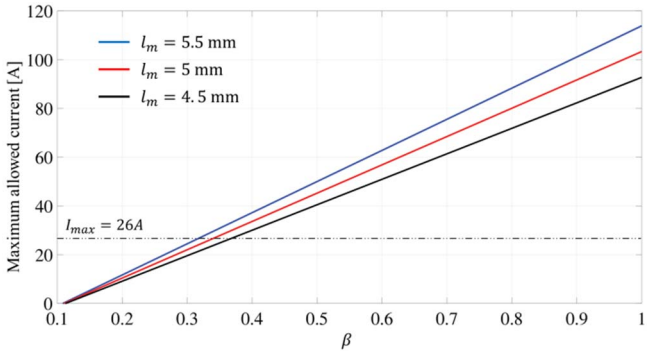

Fig. 7. Relationship among β, l_m and maximum allowed current

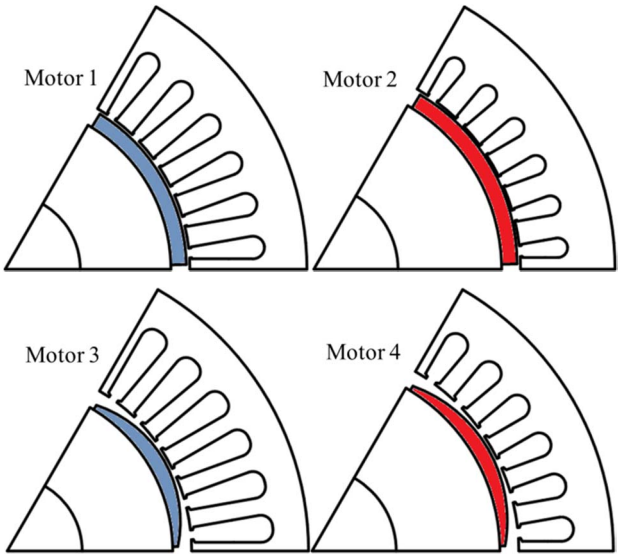

Fig. 8. Model view from parametric planes in Fig.4

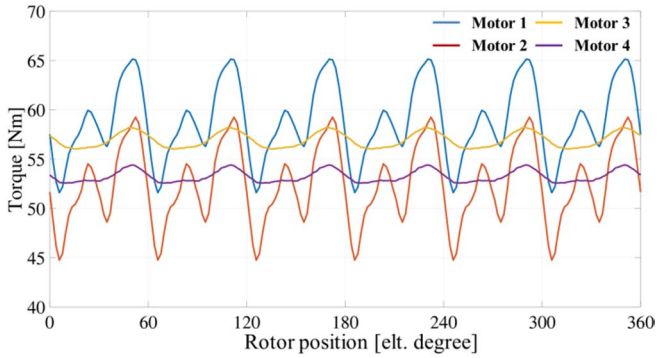

Fig. 9. Torque waveforms of the four motors

model and FEA results are reported in Table III, the torque ripple is measured by peak-peak value.

From the table, it is illustrated that the models built from parametric plane have good agreements with FEA results in terms of torque, PF, and i_q. Because the rounded shape

TABLE III COMPARISON BETWEEN PARAMETRIC PLANE AND FEA RESULTS

$l_m/g = 4.5$			Torque [Nm]	PF	i_q [A]	Torque ripple [Nm]
$\beta = 1$	$x = 0.6$	plane	59.1	0.96	26.8	-
		FEA	58.8	0.96	26.8	13.5
	$x = 0.68$	plane	51.5	0.98	21.1	-
		FEA	52.5	0.98	21.1	14.5
$\beta = 0.33$	$x = 0.6$	plane	56.8	0.93	30.7	-
		FEA	56.9	0.94	30.7	2.2
	$x = 0.68$	plane	52.3	0.96	25	-
		FEA	52.3	0.96	25	1.8
		exp.	52.2	0.95	25	-

motor has an approximate sinusoidal airgap flux distribution, the torque ripple has been significantly reduced, compared with uniform PM length motors. The torque waveforms of four motors over one entire electric period at each rated current condition are presented in Fig. 9.

Motor 4 was selected as the motor candidate since: 1) it has better PF forecast in the plane of $\beta = 0.33$ (Fig. 4b); 2) compared with uniform PM thickness, it has lower PM quantity (i.e. cost), and higher electric loading; 3) it has much better torque ripple performance at rated current condition compared with Motor 2.

C. Experimental validation

The candidate of rounded SPM motor (Motor 4) has been built and tested. Fig. 10 shows the test rig setup: it is composed by a speed control driving machine (DM), the current controlled candidate machine under test (MUT) and a data recorder [11], which stores the status of current, voltage, torque (measured by a torque meter) and speed information of MUT.

Magnetic model identification is performed, with the procedure described in [12]. During the test, also the torque over entire current domain is measured, for validation purpose. At the end of the test, the torque-current curve along Maximum Torque per Ampere (MTPA) trajectory is obtained and compared with FEA simulations and the parametric plane estimation. This comparison is reported in Fig. 11.

Table III shows the analytical, FEA and experimental results. The expected performances of torque and PF are confirmed by both FEA and experimental measurements.

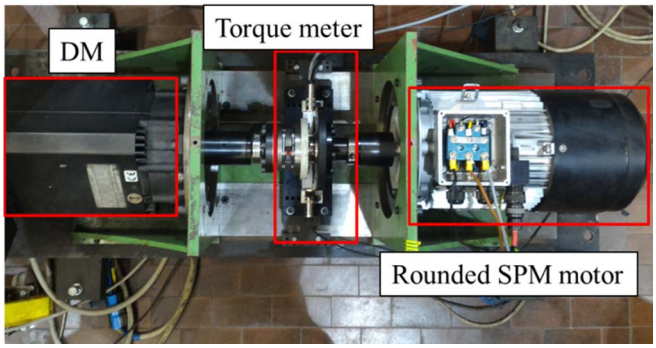

Fig. 10. Test bench for rounded SPM motor

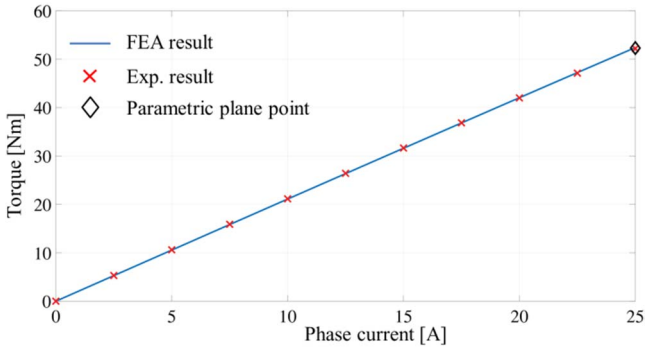

Fig. 11. Torque-current curve along MTPA route comparisons among FEA, experimental results and design plane

In terms of MTPA curve, the experimental results agree with the FEA simulations (motor speed is 300 rpm), shown in Fig. 11. Since the MTPA trajectory is almost fixed on *q* axis for SPM motor at low speed, the estimated point on parametric plane (black marked point in Fig. 11) also follows MTPA trajectory for both FEA and experimental results. The experimental results verify the accuracy of the parametric plane solution.

IV. CONCLUSION

A new parametric design method for SPM motors has been presented. The presented method applies to magnets of radial shape and also to rounded shape magnet, for cogging and torque ripple minimization. A new parametric plane, based on the intersection between torque and PF curves, is introduced. Based on that, the detailed design flowchart is illustrated. Two motor models per type are selected as examples and validated by FEA simulation results, showing good agreement with estimated performance. One qualified rounded motor was built and tested, with rounded magnets. The experimental measurements on torque and PF performance of the rounded shape SPM motor prototype is presented. They match with FEA simulations and confirm the accuracy of the presented parametric method.

REFERENCES

[1]. Z. Q. Zhu and D. Howe, "Analytical prediction of the cogging torque in radial-field permanent magnet brushless motors," in *IEEE Transactions on Magnetics*, vol. 28, no. 2, pp. 1371-1374, Mar 1992.

[2]. W. Q. Chu and Z. Q. Zhu, "Investigation of Torque Ripples in Permanent Magnet Synchronous Machines With Skewing," in *IEEE Transactions on Magnetics*, vol. 49, no. 3, pp. 1211-1220, March 2013.

[3]. N. Bianchi and S. Bolognani, "Design techniques for reducing the cogging torque in surface-mounted PM motors," in *IEEE Transactions on Industry Applications*, vol. 38, no. 5, pp. 1259-1265, Sep/Oct 2002

[4]. B. Boazzo, G. Pellegrino and A. Vagati, "Multipolar SPM Machines for Direct-Drive Application: A General Design Approach," in *IEEE Transactions on Industry Applications*, vol. 50, no. 1, pp. 327-337, Jan.-Feb. 2014.

[5]. C. Lu and G. Pellegrino, "A Simple Design Method for Surface-mounted PM Machines for Traction Application", *IEEE Energy Conversion Congress and Exposition (ECCE)*, Milwaukee, WI, Sept. 18–28, 2016,

[6]. C. Bianchini, M. Davoli, G. Pellegrino, F. Immovilli and E. Lorenzani, "Low cost PM synchronous servo-applications employing asynchronous-motor frame," *2015 IEEE Energy Conversion Congress and Exposition (ECCE)*, Montreal, QC, 2015, pp. 6090-6095.

[7]. Cupertino F. et al., "Syre - Synchronous Reluctance (machines) – evolution" [Online]. Available: http://sourceforge.net/projects/syr-e/ [Accessed: 21- Jun- 2017]

[8]. D. Meeker. "Finite Element Method Magnetics (FEMM)". [Online]. Available: http://femm.foster-miller.net [Accessed: 21- Jun- 2017]

[9]. Lipo, Thomas A. "*Introduction to AC machine design*", Wisconsin Power Electronics Research Center, University of Wisconsin, 2014

[10]. Pyrhonen, Juha, "*Design of rotating electrical machines*", John Wiley & Sons, 2009

[11]. https://www.hbm.com/en/3868/data-recorder-gen3i-and-transient-recorder/ [Accessed: 21-Jun-2017]

[12]. E. Armando, P. Guglielmi, G. Pellegrino and R. Bojoi, "Flux Linkage Maps Identification of Synchronous AC Motors Under Controlled Thermal Conditions," *2017 IEEE International Electric Machines and Drives Conference (IEMDC)*, Miami, FL, 2017.